Measurements of the properties of D-meson decays

R. H. Schindler,* M. S. Alam,† A. M. Boyarski, M. Breidenbach, D. L. Burke, J. Dorenbosch,* J. M. Dorfan,
G. J. Feldman, M. E. B. Franklin, G. Hanson, K. G. Hayes,* T. Himel,* D. G. Hitlin,‡ R. J. Hollebeek, W. R. Innes,
J. A. Jaros, P. Jenni,* R. R. Larsen, V. Lüth, M. L. Perl, B. Richter, A. Roussarie, D. L. Scharre, R. F. Schwitters,§
J. L. Siegrist, H. Taureg,* M. Tonutti,‖ R. A. Vidal, J. M. Weiss, and H. Zaccone�ε

Stanford Linear Accelerator Center, Stanford University, Stanford, California 94305

G. Abrams, C. A. Blocker,§ A. Blondel, W. C. Carithers, W. Chinowsky, M. W. Coles, S. Cooper,** W. E. Dieterle,
J. B. Dillion, M. W. Eaton, G. Gidal, G. Goldhaber, A. D. Johnson, J. A. Kadyk, A. J. Lankford, R. E. Millikan,
M. E. Nelson, C. Y. Pang, J. F. Patrick, J. Strait, G. H. Trilling, E. N. Vella, and I. Videau††

Lawrence Berkeley Laboratory and Department of Physics, University of California, Berkeley, California 94720
(Received 11 February 1981)

We present a study of the decay properties of charmed D mesons produced near the peak of the $\psi'''(3770)$ resonance in e^+e^- annihilation. Branching fractions for nine Cabibbo-favored and three Cabibbo-suppressed decay modes are presented along with upper limits on one additional Cabibbo-favored and four additional Cabibbo-suppressed decay modes. A study of $K\pi\pi$-decay-mode Dalitz plots reveals a large quasi-two-body pseudoscalar-vector component for the D^0 decays and an apparent nonuniform population on the Dalitz plot for the D^+ decay into $K^-\pi^+\pi^+$. Using tagged events, we measure the charged-particle multiplicity and strange-particle content of D decays. A measurement of the D^+ and D^0 semileptonic decay fractions indicates that the D^+ has a significantly longer lifetime than the D^0.

I. INTRODUCTION

The charmed D mesons were discovered in e^+e^- annihilation[1] several years ago and have subsequently been detected in neutrino-,[2-4] hadron-,[5] and photon-induced[6-8] reactions. Detailed information on their decay properties has come predominantly from e^+e^- experiments near the threshold for D-meson production, where the cross section is large compared to background processes.[9-23]

We present a study of the properties of D-meson final states, obtained from a sample of about 900 reconstructed decays. The data were obtained with the Mark II magnetic detector at the Stanford Linear Accelerator Center e^+e^- storage ring SPEAR. The center-of-mass energy ($E_{\text{c. m.}}$) was 3.771 ± 0.001 GeV, which is near the peak of the $\psi''(3770)$ resonance.[18,24,25] The proximity of this resonance to the $D\bar{D}$ threshold results in low-momentum two-body D production, which permits a reduction of background through kinematic constraints and improved particle identification. The data sample contained 50 000 hadronic events and had an integrated luminosity of 2850 nb^{-1}.

In Sec. II we present some of the initial theoretical expectations for charmed-meson decay. Section III contains a description of the detector. In Sec. IV we summarize the measurements of D-production cross sections at the ψ'' resonance. Section V contains measurements on exclusive final states including measurements of branching fractions for Cabibbo-favored and -suppressed

hadronic decay modes, studies of $K\pi\pi$-decay-mode Dalitz plots, and measurements of the D^0 and D^+ mass. In Sec. VI we present a study of inclusive properties of D-meson decays including the charged-particle multiplicities and strange-particle content. Also included is a measurement of semileptonic branching fractions of neutral and charged D's, which allows a determination of their relative lifetimes. Finally, Sec. VII contains a comparison of the experimental results with early theoretical models and a discussion of the later modifications to these models that have been proposed to account for the discrepancies.

II. INITIAL THEORETICAL EXPECTATIONS

The existence of the charmed quark was postulated theoretically by Glashow, Iliopoulos, and Maiani (GIM) to explain the absence of strangeness-changing neutral currents and to achieve lepton-hadron symmetry.[26,27] A manifestation of the charmed quark would be the existence of three new mesons stable against strong and electromagnetic decay. There would be an isodoublet of D mesons, the D^0 with $c\bar{u}$ quark content and the D^+ with $c\bar{d}$ quark content, and an isosinglet F^+ meson with $c\bar{s}$ quark content.[27,28]

Early discussions[28-32] of the properties of weak hadronic decays of charmed particles were based on the light-quark-spectator model. In this model the Cabibbo-allowed decay process is envisioned to arise from a c-quark-to-s-quark transition via the omission of a virtual W^+ boson,

which then decays to a $u\bar{d}$ quark pair, as illustrated in Fig. 1. The accompanying light quark is not directly involved in the decay, hence the term "spectator." An immediate consequence of this picture is that the lifetimes of the three charmed mesons should be about the same.[32]

A second tenet of the models first proposed to explain charmed-particle decays is that hard-gluon renormalization effects can be accounted for in leading-logarithm approximation by renormalization-group techniques.[30] Thus the renormalized weak Hamiltonian governing these decays can be written as

FIG. 1. Light-quark-spectator diagram for Cabibbo-favored charmed-meson decay.

$$H_{\text{eff}} = \frac{G}{2\sqrt{2}} \cos^2\theta_c \{(f_+ + f_-)[\bar{c}^a\gamma_\mu(1-\gamma_5)s_a][\bar{d}^b\gamma_\mu(1-\gamma_5)u_b] + (f_+ - f_-)[\bar{c}^a\gamma_\mu(1-\gamma_5)u_a][\bar{d}^b\gamma_\mu(1-\gamma_5)s_b]\},$$ (1)

where a and b are summed color indicies. In the absence of strong interactions $f_+ = f_- = 1$.

The short-distance renormalization effects are incorporated in the coefficients $f_\pm$, whose values depend largely on the assumed magnitude of the strong-coupling constant α_s. For values of α_s in the range 0.2 to 0.7, f_- varies from 1.4 to 2.3 and $f_+ = f_-^{-1/2}$ varies from 0.85 to 0.66. The f_- coefficient is an enhancement factor for the part of the amplitude which transforms as a sextet under SU(3) and the f_+ coefficient is a suppression factor for the part of the amplitude which transforms as a 15-plet.

The fraction of semileptonic decays of charmed mesons should be identical and given by[32]

$$\frac{\Gamma(D \to e^+\nu + \text{hadrons})}{\Gamma(D \to \text{all})} = \frac{1}{2 + 2f_+^2 + f_-^2}$$

$$= 0.12 \text{ to } 0.185 .$$ (2)

This value is 0.20 in a free-quark model ($f_+ = f_- = 1$).

These ideas and the assumption that gluon interactions do not change the color structure of final states lead to predictions among the nonleptonic decay modes. A particularly dramatic example is[30]

$$\frac{\Gamma(D^0 \to \bar{K}^0\pi^0)}{\Gamma(D^0 \to K^-\pi^+)} = \frac{1}{2}\left(\frac{2f_+ - f_-}{2f_+ + f_-}\right)^2 \lesssim \frac{1}{27} .$$ (3)

This prediction of a large difference in the relative decay fractions for these two modes results mainly from a suppression due to a mismatch of colors in the dominant diagram for $D^0 \to \bar{K}^0\pi^0$.

First-order Cabibbo-suppressed decays occur by either the c quark decaying to a d quark, as illustrated in Fig. 2(a), or by the virtual W boson decaying to a $u\bar{s}$ quark pair, as illustrated in Fig. 2(b). In a four-quark model each process occurs at a level of $\tan^2\theta_c(\approx 0.05)$ of the dominant Cabibbo-
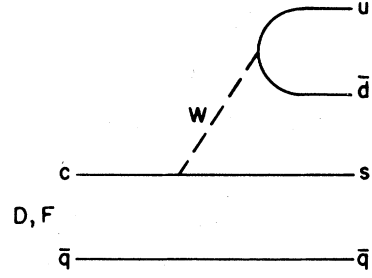
allowed process, shown in Fig. 1. In a six-quark model, using the usual Kobayashi-Maskawa notation,[33] the $\tan^2\theta_c$ is replaced by

$$\frac{\sin^2\theta_1\cos^2\theta_2}{|\cos\theta_1\cos\theta_2\cos\theta_3 - \sin\theta_2\sin\theta_3 e^{i\delta}|^2}$$

in the process depicted by Fig. 2(a), and by $\tan^2\theta_1 \cos^2\theta_3$ in the process depicted by Fig. 2(b).

In general, specific predictions for final states cannot be made solely from a knowledge of these mixing angles; however, in the limit of four quarks and exact SU(3) symmetry,[29]
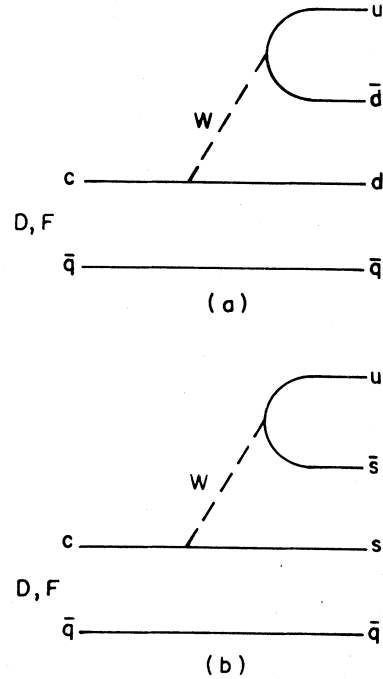

FIG. 2. Light-quark-spectator diagrams for Cabibbo-suppressed charmed-meson decay.

$$\Gamma(D^0 \to \pi^-\pi^+) = \Gamma(D^0 \to K^-K^+)$$

$$= \tan^2\theta_C \Gamma(D^0 \to K^-\pi^+) . \qquad (4)$$

III. DETECTOR

Figures 3 and 4 show expanded three-dimensional and cross-sectional views of the Mark II detector. Starting at the interaction region a particle will first traverse a corrugated stainless-steel vacuum pipe and a set of trigger scintillation counters, which together comprise about 0.05 radiation lengths (r.l.) of material. It will then encounter a 16-layer drift chamber, one of 48 time-of-flight (TOF) counters, and a 1.4-r.l. aluminum solenoidal coil, which produces a 0.42-T axial magnetic field. Beyond the coil are eight lead–liquid-argon electromagnetic shower-counter modules and two or three layers of muon identifiers, each layer consisting of 23 to 30 cm of iron and a set of proportional tubes.

Charged tracks are reconstructed from hits in the 16 cylindrical drift-chamber layers which, for this analysis, provide solid-angle coverage over 76% of 4π sr. The azimuthal coordinates of charged tracks are measured to an rms accuracy of approximately 220 μm at each layer. The polar coordinates are determined from the 10 stereo layers at $\pm3°$ to the beam axis. When a vertex constrained fit can be made, the charged-particle rms momentum resolution can be expressed as

$$\delta p/p = [(0.015)^2 + (0.005p)^2]^{1/2} , \qquad (5)$$

where p is the momentum in GeV/c. Without this constraint the momentum-dependent term is doubled.

The TOF scintillation counters which surround the drift chamber provide timing information over 75% of 4π sr. Each TOF counter is a 2.54-cm-thick Pilot F scintillator, 3.44 m long, and is viewed on each end by Amperex XP 2230 photomultiplier tubes through Lucite light guides. The
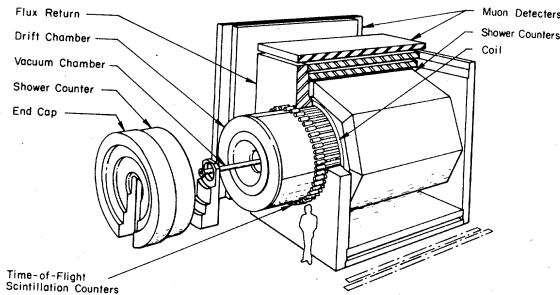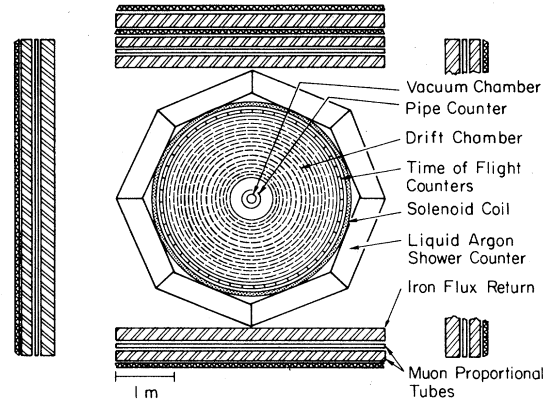

FIG. 4. Cross-sectional view of the Mark II magnetic detector. The incident e^+ and e^- beams are normal to the plane of the figure.

system is calibrated using isochronous light pulses from an N_2 flashtube, brought to the center of each counter through 10-m-long quartz optical fibers. Signals from the tubes are fed to 12-bit time-to-digital converters (TDC's) and analog-to-digital converters (ADC's), the latter allowing a pulse height correction to be made. These slewing corrections are calculated off-line from Bhabha-scattered electrons and allow us to obtain a system resolution of 315 ps for hadrons for this data sample.

The lead–liquid-argon shower-counter modulus which surround the solenoid are used to detect photons and identify high-energy electrons. The modules are approximately 14 r.l. in depth and cover 64% of 4π sr. The rms energy resolution for photons above 500 MeV in the calorimeter is approximately $12\%/\sqrt{E}$ (GeV), deviating somewhat at lower energies. The angular resolution for low-energy photons is approximately 8 mrads.

The detector trigger employs a track-finding hardware processor requiring at least one track to traverse the entire drift chamber and an additional track to cross at least three of the five inner layers. Since all D decays that we investigate have at least two charged tracks which satisfy these requirements, the trigger efficiency does not depend on how the other D in the event decays.

The luminosity of the sample is monitored by a pair of small-angle scintillator and shower-counter telescopes. These counters are positioned at 22 mrad from the beam axis, and identify Bhabha-scattered electrons. The counters are calibrated against larger-angle Bhabha events measured in the fiducial volume of the drift chamber and lead–liquid-argon calorimeter.

Additional details of the drift chamber, trigger electronics, and calorimeters are presented elsewhere.[34-37]

FIG. 3. Expanded, cut-away view of the Mark II magnetic detector.

IV. THE $\psi''(3770)$ RESONANCE

The data were collected near the peak of the $\psi''(3770)$ resonance.[18,24,25] Because it lies only 80 MeV above the $\psi'(3684)$ but has a total width about two orders of magnitude greater, we attribute its width solely to the strong decay of the resonance to the newly opened $D\bar{D}$ channel. If the ψ'' has a unique isospin then it couples equally within phase-space factors to pairs of charged and neutral D mesons. Thus, a measurement of the ψ'' resonance and background permits an evaluation of the inclusive charmed-meson production cross section.

A fine scan over the ψ'' was made to remeasure the resonance parameters.[25] The inclusive cross sections for D production at $E_{c.m.} = 3.771$ GeV were found to be

$$\sigma_{D^0} + \sigma_{\bar{D}^0} = 8.0 \pm 1.0 \pm 1.2 \text{ nb},$$

$$\sigma_{D^+} + \sigma_{D^-} = 6.0 \pm 0.7 \pm 1.0 \text{ nb}.$$

(6)

The values given here are observed cross sections uncorrected for radiative effects, which allows their direct use in branching-ratio determinations. The first error is statistical and the second is our estimate of the systematic uncertainty in the overall scale, the assumptions that go into the fit of the resonance and background shape, and the division of phase space between the $D^0\bar{D}^0$ and D^+D^- final states.

V. EXCLUSIVE FINAL STATES OF D MESONS

A. Cabibbo-favored decays

We present in this section measurements of the cross section times branching ratio (σB) at $E_{c.m.} = 3.771$ GeV for final states containing either one charged or one neutral kaon. In addition, from the inclusive D-meson production cross sections given in Sec. IV, estimates of absolute branching ratios are obtained. For clarity, D^0 and D^+ will be used to refer both to the meson state and its charge conjugate.

For the reconstruction of final states all charged tracks are required to come within 4 cm radially and ± 15 cm longitudinally of the measured beam crossing point. To improve momentum resolution multiprong events are constrained to pass through the primary interaction point, after secondary vertices (K_S^0, Λ) have been removed. Measurements of charged-particle momenta are corrected for dE/dx losses in material traversed before entering the drift chamber.

The reconstruction techniques used for neutral kaons and pions are described in Ref. 34. Briefly, neutral kaons are identified through their $\pi^+\pi^-$ decay and selected by cuts in both dipion mass

and direction. To reduce combinatorial background, the decay distance projected into the plane normal to the incident beams is required to be greater than 2 mm. The resulting $\pi^+\pi^-$ mass spectrum is shown in Fig. 5(a). The observed rms K^0 resolution is 6 MeV/c^2, and we employ a mass cut of ± 18 MeV/c^2 as indicated.

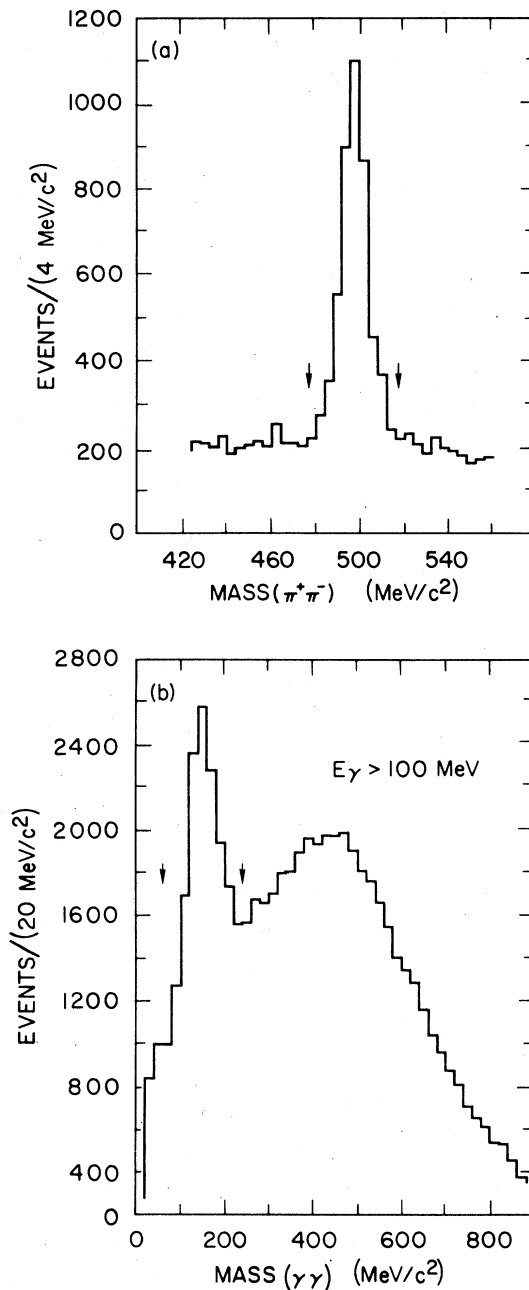Neutral pions are reconstructed from pairs of

FIG. 5. (a) Dipion mass spectrum in the region of the K_S^0 and (b) diphoton mass spectrum in the region of the π^0. Mass cuts that were used to isolate K_S^0 and π^0 are indicated by arrows.

photons, each with an energy greater than 100 MeV. The resulting $\gamma\gamma$ mass spectrum Fig. [5(b)] has an rms π^0 peak resolution of about 25 MeV/c^2 and background comparable to the signal. The mass cut indicated is chosen to reduce the loss of signal in the tails of the peak. Both K_S^0 and π^0 candidates must satisfy a one-constraint fit in which the momenta and angles of the tracks are adjusted to obtain the correct masses. For the π^0, the good angular resolution for photons is an important constraint in the fit.

Charged particles are identified with the time-of-flight (TOF) system. For each track having a recorded TOF, a normalized weight is calculated for the π-, K-, and p-mass hypotheses.[38] These weights are based on measured momentum, path length, TOF, and TOF resolution. Tracks are assigned a particle type corresponding to the hypothesis with the highest weight. Tracks lacking TOF information or having TOF inconsistent with that expected for a π, K, or p assignment are called pions. Because D mesons are produced with momenta below 300 MeV/c, only the most energetic (two-body) decay products have

momenta exceeding 1 GeV/c. Since the average flight path is about 1.75 m, π-K separation exceeds 2.0 standard deviations for the decay products of the D meson in any channel.

Since the production of D mesons at the $\psi''(3770)$ occurs only through $D\overline{D}$ final states, the mass resolution in most channels can be further improved by constraining the sum of the measured energies to that of the beam (E_b). Thus for particle combinations with measured total energy close to E_b (within 40−60 MeV), we plot the quantity

$$M_c = (E_b^2 - p^2)^{1/2}. \tag{7}$$

The improvement in resolution is obtained because of the small spread in E_b (~1.3 MeV) and the small size of the D momenta (p) and errors relative to M_c. The D^+ and D^0 have momenta of ~255 and 288 MeV/c, respectively, with typical momentum uncertainties less than 15 MeV/c. For decays involving a single π^0, the constraints of π^0 mass, photon direction, and beam energy can be imposed simultaneously to evaluate p and compute M_c as in Eq. (7).

In Figs. 6 and 7, mass plots in the variable M_c are shown for final states with no π^0's. Figure 8 shows channels containing single π^0. These plots provide evidence for the previously un-
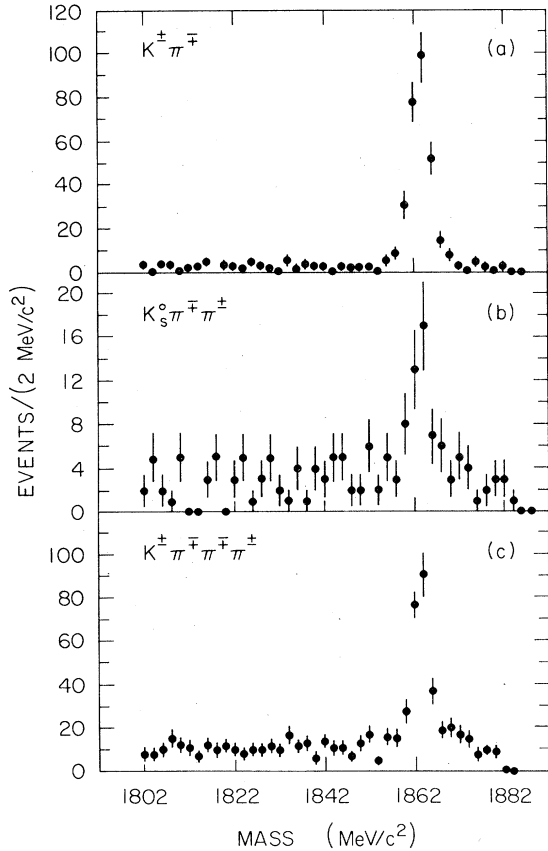

FIG. 6. Beam−energy−constrained mass spectra for (a) $K^-\pi^+$, (b) $K_S^0\pi^+\pi^+$, and (c) $K^-\pi^+\pi^+\pi^-$ combinations.
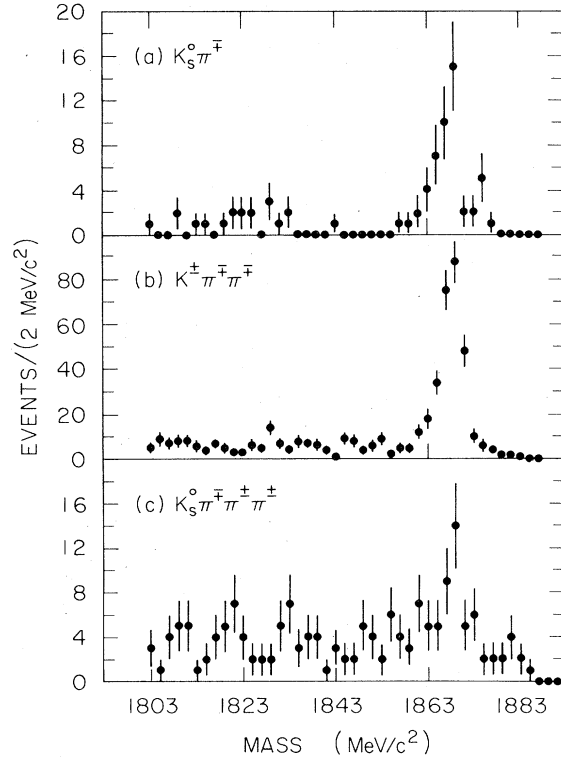

FIG. 7. Beam−energy−constrained mass spectra for (a) $K_S^0\pi^+$, (b) $K^-\pi^+\pi^+$, and (c) $K_S^0\pi^-\pi^+\pi^+$ combinations.
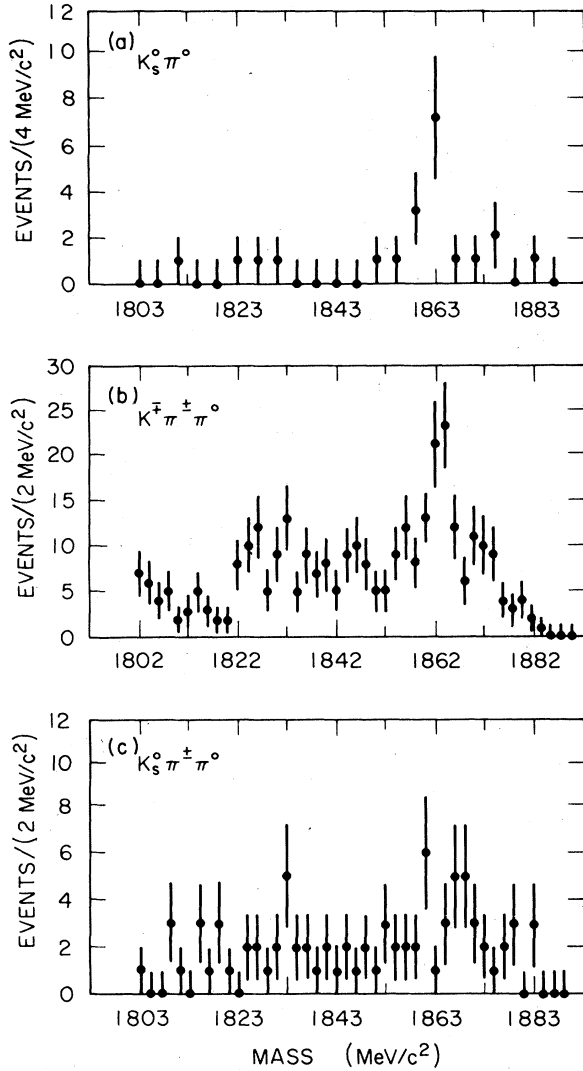
FIG. 8. Beam-energy-constrained mass spectra for (a) $K_S^0\pi^0$, (b) $K^-\pi^+\pi^0$, and (c) $K_S^0\pi^+\pi^0$ combinations.

measured decays of the D^0 into $\overline{K}^0\pi^0$ and the D^+ into $\overline{K}^0\pi^+\pi^+\pi^-$, as well as for a number of previously measured channels. With less significance there is an indication of the decay $D^+ \rightarrow \overline{K}^0\pi^+\pi^0$ in Fig. 8.

To determine the detection efficiencies for these final states an extensive Monte Carlo simulation of the detector is employed. $D\overline{D}$ pairs are generated using the production angular distribution for a pair of pseudoscalar mesons and are allowed to decay to the mode under study. The decay products are tracked in the detector and are themselves allowed to decay, generating raw data which is then passed through the standard tracking, vertex-finding, and event-identification algorithms used to generate actual data summary tapes. These Monte Carlo tapes are then analyzed as data in order to determine efficiencies. The Monte Carlo is designed to represent as closely as possible the response of the detector. As an example, the generation of drift-chamber data from charged particles incorporates multiple Coulomb scattering, dE/dx and radiative energy loss, nuclear absorption and scattering, non-linearities in the drift-chamber distance-to-time relation, and δ rays, as well as observed correlations between adjacent cells. The primary-vertex distribution is determined from Bhabha-scattering events. Photons are assigned detection efficiencies and position and energy resolutions previously found with an electromagnetic-shower Monte Carlo simulation.[39] The results were found to agree with measured values obtained by performing kinematic fits to multipion decays of the $\psi(3095)$ containing a single π^0.[37] In the Monte Carlo calculation all decays were assumed to follow a uniform phase-space distribution, except the channels $\overline{K}^0\pi^+\pi^-$ and $K^-\pi^+\pi^0$, where the measured resonant substructure (see next subsection) was employed.

TABLE I. Cross section times branching fraction (σB) and branching fraction (B) for Cabibbo-favored D decays. The results quoted refer to the sum of the mode and its charge conjugate. The error on the number of signal events includes the uncertainty in the background shape. The $K\pi\pi$ modes include the contribution from two-body pseudoscalar-vector decays discussed in Sec. VB. The upper limits are at the 90% confidence level.

Mode	Signal	Efficiency	σB (nb)	$B(\%)$
$K^-\pi^+$	263.0 ± 17.0	0.386	0.24 ± 0.02	3.0 ± 0.6
$\overline{K}^0\pi^0$	8.5 ± 3.7	0.017	0.18 ± 0.08	2.2 ± 1.1
$\overline{K}^0\pi^+\pi^-$	32.0 ± 7.7	0.037	0.30 ± 0.08	3.8 ± 1.2
$K^-\pi^+\pi^0$	37.2 ± 10.0	0.019	0.68 ± 0.23	8.5 ± 3.2
$K^-\pi^+\pi^+\pi^-$	185.0 ± 18.0	0.095	0.68 ± 0.11	8.5 ± 2.1
$\overline{K}^0\pi^+$	35.7 ± 6.7	0.090	0.14 ± 0.03	2.3 ± 0.7
$K^-\pi^+\pi^+$	239.0 ± 17.0	0.221	0.38 ± 0.05	6.3 ± 1.5
$\overline{K}^0\pi^+\pi^0$	9.5 ± 5.5	0.004	0.78 ± 0.48	12.9 ± 8.4
$\overline{K}^0\pi^+\pi^+\pi^-$	21.0 ± 7.0	0.015	0.51 ± 0.18	8.4 ± 3.5
$K^-\pi^+\pi^+\pi^-\pi^+$	< 11.5	0.021	< 0.23	< 4.1

TABLE II. A comparison of σB measured by this experiment and the lead-glass-wall (Mark I) experiment (Refs. 15 and 16).

Mode	σB (nb) (This experiment) $E_{c.m.} = 3.771$ GeV	σB (nb) (Refs. 15 and 16) $E_{c.m.} = 3.774$ GeV	Difference
$K^-\pi^+$	0.24 ± 0.02	0.25 ± 0.05	-0.01 ± 0.05
$\bar{K}^0\pi^+\pi^-$	0.30 ± 0.08	0.46 ± 0.12	-0.16 ± 0.14
$K^-\pi^+\pi^0$	0.68 ± 0.23	1.4 ± 0.6	-0.72 ± 0.64
$K^-\pi^+\pi^+\pi^-$	0.68 ± 0.11	0.36 ± 0.10	0.32 ± 0.15
$\bar{K}^0\pi^+$	0.14 ± 0.03	0.14 ± 0.05	0.00 ± 0.06
$K^-\pi^+\pi^+$	0.38 ± 0.05	0.36 ± 0.06	0.02 ± 0.08

Table I summarizes the results for the D^0 and D^+ channels shown. An upper limit on the five-body D^+ decay to $K^-\pi^+\pi^+\pi^+\pi^-$ is also included. The quoted errors include all systematic sources taken in quadrature with the statistical errors obtained from fits to the spectra.

A comparison of σB for all previously reported[15,16] decay modes is given in Table II and indicates general agreement. In particular, it is only for the $K^-\pi^+\pi^+\pi^-$ mode that we observe a deviation greater than two standard deviations in the combined errors. The absolute branching ratios of Table I differ from Refs. 15 and 16 predominantly in the normalization of σ_{D^0} and σ_{D^+}. The values we obtain from Eq. (6) are approximately 30% smaller than those employed in Refs. 15 and 16.

B. $D \to K\pi\pi$ Dalitz plots

We describe next the measurement of the Dalitz-plot distributions for $K^-\pi^+\pi^0$ and $\bar{K}^0\pi^+\pi^-$ decays of the D^0 and the $K^-\pi^+\pi^+$ decay of the D^+. We find that the three-body decays of the D^0 show significant contributions from the quasi-two-body decay modes containing a vector particle (ρ or K^*) and a pseudoscalar (K or π), while the D^+ shows very little structure of this kind. These decays are of particular theoretical interest, for as two-body modes they provide simple probes of the $I = \frac{1}{2}$ and $I = \frac{3}{2}$ couplings of the weak-hardronic current in charm decays.

To determine the resonant substructure of each decay, we performed a maximum-likelihood fit to the data in the Dalitz plot using a density function representing the allowed final-state channels and background. Corrections for detector acceptance are made at each point.

In the fit, the ρ and K^* amplitudes have been represented as p-wave Breit-Wigner line shapes, with energy-dependent widths and the appropriate decay angular distribution. The general fitting technique that we employed is described in Ref. 40.

We treated the nonresonant components (either pure three-body decays or background events in the D-meson sample) separately in the D^0 fits. The pure three-body component of the D^0 decays was assumed to be produced uniformly over the Dalitz plot, while the shape used to represent background events was derived by smoothing the low-mass sideband (1800–1850 MeV/c^2). For the D^+, we found excellent agreement between efficiency-corrected uniform phase space and the low-mass sideband, and used this representation for both signal and background. In each case we examined events in the sideband for evidence of K^* and ρ and found no indication of significant resonant production there. In the fit, we allow the pure three-body component of the decay to vary, while the background contribution is constrained to its measured magnitude and error.

The amplitudes of all indistinguishable final states that are accessible in each decay are allowed to interfere, with the independent relative phases being varied only when statistically significant improvements in the fit are observed. In general the fits are not sensitive to the effects of interference, both because of low statistics and because the decays appear dominated by single channels.

1. $\bar{K}^0\pi^+\pi^-$ and $K^-\pi^+\pi^0$

Figure 9(a) shows the Dalitz plot for the $\bar{K}^0\pi^+\pi^-$ decay mode. This plot contains 52 events of which 33% are estimated to be background.[41] There are significant populations in the K^* bands centered around 0.79 (GeV/c^2)^2. Conservation of angular momentum requires that the vector-particle decay products have a $\cos^2\theta$ angular distribution, where θ is the angle between the direction of a decay product and the direction of the pseudoscalar particle in the vector particle's center-of-mass frame. This leads to the clustering of events at the ends of the K^* bands, which is observed in Fig. 9(a). There is no significant indication of a $\bar{K}^0\rho^0$ signal. Figure 9(d) shows the lower-mass $\bar{K}^0\pi^+$ projection of the Dalitz plot with
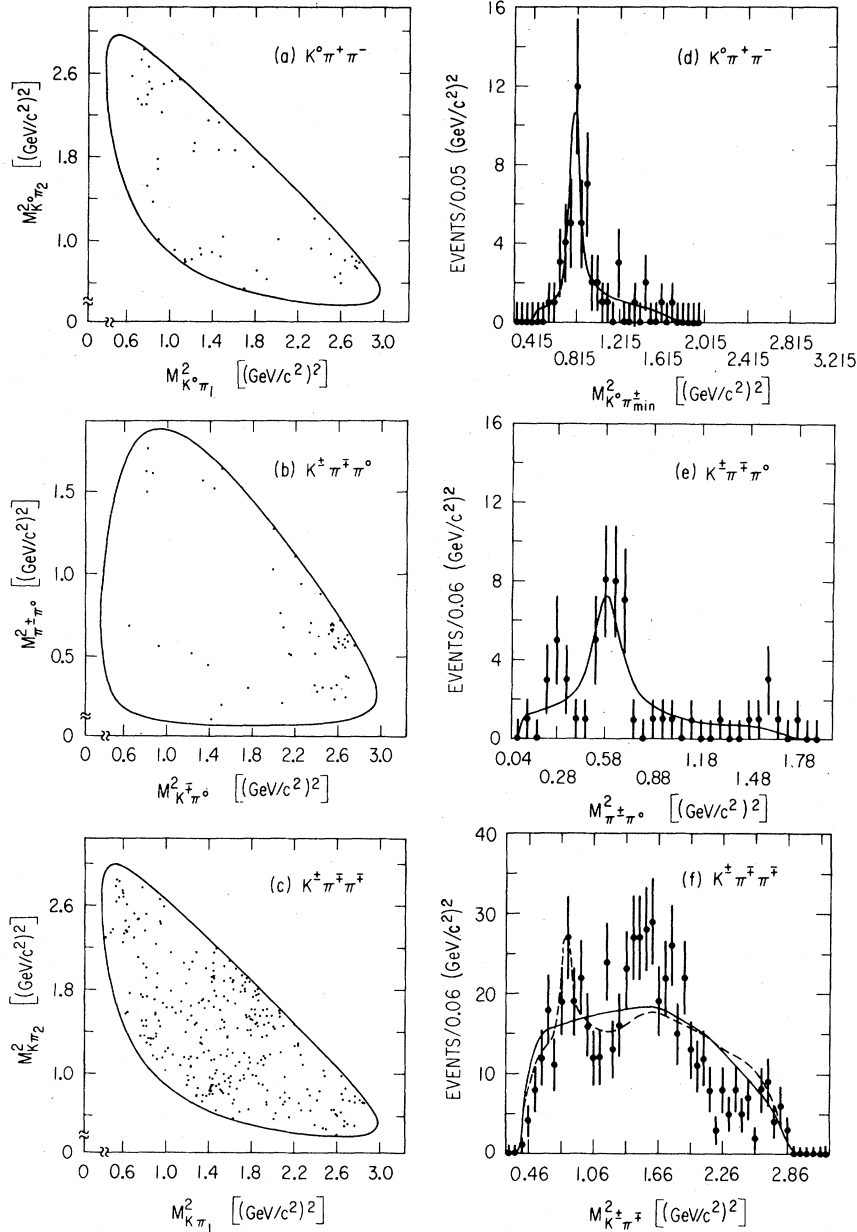
FIG. 9. Dalitz plots for (a) $D^0 \to K_S^0 \pi^+ \pi^-$, (b) $D^0 \to K^- \pi^+ \pi^0$, and (c) $D^+ \to K^- \pi^+ \pi^+$, and (d)–(f) projections of these plots. The solid curves in (d) and (e) represent the fits discussed in the text. In (f) the solid curve represents the shape expected for a uniform distribution on the Dalitz plot folded with the acceptance. The dashed curve represents the shape which results from a 15% $K^{*0} \pi^+$ mode plus a constant matrix element.

a smooth curve representing the fitted solution. The results of the fit are summarized in Table III.

Figure 9(b) shows the Dalitz plot for the $K^- \pi^+ \pi^0$ decay mode. Here there are 56 events of which 43% are estimated to be background.[41] There is a large enhancement in the ρ^+ band centered near 0.58 $(\text{GeV}/c^2)^2$. The concentration of events on the right side of the plot is caused by the rapidly

changing π^0 acceptance. This changing π^0 acceptance partially obscures the expected angular distribution in the ρ^+ band, as well as the neutral and charged K^* signals that may be present. Figure 9(e) shows the $\pi^+ \pi^0$-mass-squared projection of the Dalitz plot and a curve representing the fitted solution. The results of the fit are summarized in Table III.

The results given in Table III are recast as branching fractions in Table IV. Table IV was

TABLE III. Results of fits to $D^0 \to K\pi\pi$ Dalitz plots. The values represent the fraction of a channel in the absence of interference. They do not sum to unity because of interference effects (see Ref. 40). The statistical error is derived from the likelihood function in the fitting procedure. The systematic error is the estimated uncertainty from the Monte Carlo statistics, the acceptance calculation, and assumptions about backgrounds and resonance line shapes.

Decay mode	Channel	Fraction	Statistical error	Systematic error
$\overline{K}^0\pi^+\pi^-$	$K^{*-}\pi^+$	0.70	$+0.15$ -0.17	$+0.05$ -0.06
	$\overline{K}^0\rho^0$	0.02	$+0.14$ -0.02	±0.02
	nonresonant	0.30	$+0.23$ -0.21	±0.05
$K^-\pi^+\pi^0$	$K^-\rho^+$	0.85	$+0.11$ -0.15	$+0.09$ -0.10
	$\overline{K}^{*0}\pi^0$	0.11	$+0.14$ -0.09	±0.10
	$\overline{K}^{*-}\pi^+$	0.07	$+0.07$ -0.06	$+0.05$ -0.02
	nonresonant	0.00	$+0.21$ -0.00	$+0.05$ -0.00

constructed by multiplying the resonant fractions from Table III by the branching fractions given in Table I and by dividing, when necessary, by the appropriate K^* branching fractions. The $D^0 \to K^{*-}\pi^+$ branching fraction has been measured in both the $\overline{K}^0\pi^+\pi^-$ and $K^-\pi^+\pi^0$ modes. A best fit to both measurements yields a branching fraction of $(3.4 \pm 1.4)\%$.

2. $K^-\pi^+\pi^+$

Figure 9(c) shows the Dalitz plot for $D^+ \to K^-\pi^+\pi^+$. There are 292 events including an estimated background of 12%.[41] Detection efficiency for the D^+ is quite uniform across the plot, dropping only near the three corners where π and K momenta fall below about 100 MeV/c. These

TABLE IV. Summary of pseudoscalar-vector branching fractions (%) derived from the observed $\overline{K}_0\pi^+\pi^-$ and $K^-\pi^+\pi^-$ decay modes. The upper limit is at the 90% confidence level.

Mode	$\overline{K}^0\pi^+\pi^-$	$K^-\pi^+\pi^0$
Nonresonant	1.1 ± 0.9	<2.4
$K^{*-}\pi^+$	4.0 ± 1.6	$1.8^{+2.3}_{-1.8}$
$\overline{K}^0\rho^0$	$0.1^{+0.6}_{-0.1}$	
$\overline{K}^{*0}\pi^0$		$1.4^{+2.3}_{-1.4}$
$K^-\rho^+$		$7.2^{+3.0}_{-3.1}$

data, which have more events and substantially less background than previous samples of this decay mode, show the first evidence for a non-uniform population on the Dalitz plot.[42] A simple test of uniformity was made by dividing the plot into eleven well-populated regions and by comparing the observed number of events in each region with the number expected from the hypothesis of a uniform decay distribution. The hypothesis fails statistically with a χ^2 of 83 for 10 degrees of freedom.

Figure 9(f) shows the $K^-\pi^+$-mass-squared projection. The solid curve indicates the shape expected for a uniform-phase-space decay, and the dashed curve indicates the shape for a decay containing 15% $\overline{K}^{*0}$ in addition to a uniform component. The $\overline{K}^{*0}$ curve includes the effect of the constructive interference of the two possible $K^-\pi^+$ combinations. There are large deviations from uniform phase space but no significant $\overline{K}^{*0}$ signal.

Because we are unable to fit the distribution on the Dalitz plot, we present only a conservative upper limit on the $\overline{K}^{*0}\pi^+$ channel by assuming that all the events in the $\overline{K}^{*0}$-mass-squared region, 0.685 to 0.905 $(\text{GeV}/c^2)^2$, are due to this channel. At the 90% confidence level the fraction of the $K^-\pi^+\pi^+$ mode in the $\overline{K}^{*0}\pi^+$ channel is less than 0.39. Using the $K^-\pi^+\pi^+$ branching fractions from Table I and dividing by the $\overline{K}^{*0}$ branching fraction, we obtain

$$B(D^+ \to \overline{K}^{*0}\pi^+) < 3.7\% \qquad (8)$$

at the 90% confidence level.

3. $\overline{K}^0\rho^+$

The only pseudoscalar-vector D decay involving K, K^*, π, or ρ that we have not discussed is $D^+ \to \overline{K}^0\rho^+$. In principle this decay can be measured in the $K_S\pi^+\pi^0$ channel, but this is not practical since we have a total of only 9.5 ± 5.5 $K_S\pi^+\pi^0$ events. We can, however, obtain a lower bound on the branching fraction for this decay mode by using measurements of other modes and the isospin structure of D decays. The amplitudes A for the decays $D^0 \to \overline{K}^0\rho^0$, $D^0 \to K^-\rho^+$, and $D^+ \to \overline{K}^0\rho^+$ are related by the triangle relation

$$A(D^0 \to K^-\rho^+) + \sqrt{2}\,A(D^0 \to \overline{K}^0\rho^0) - A(D^+ \to \overline{K}^0\rho^+) = 0. \qquad (9)$$

This yields an inequality for the branching fractions B,

$$B(D^+ \to \overline{K}^0\rho^+) \geq \frac{\tau_{D^+}}{\tau_{D^0}}\{[B(D^0 \to K^-\rho^+)]^{1/2}$$
$$- [2B(D^0 \to \overline{K}^0\rho^0)]^{1/2}\}^2, \qquad (10)$$

where the τ's are the lifetimes of the D mesons. Using the branching fractions from Table IV and

the likelihood functions for τ_{D^+}/τ_{D^0} to be discussed in Sec. VI C, we obtain

$$B(D^+ \to \overline{K}{}^0\rho^+) > 1.6\% \tag{11}$$

at the 90% confidence level using this experiment's determination of τ_{D^+}/τ_{D^0}, or

$$B(D^+ \to \overline{K}{}^0\rho^+) > 5.0\% \tag{12}$$

at the 90% confidence level using the world data for τ_{D^+}/τ_{D^0}.

C. Cabibbo-suppressed decays

In this section we present measurements on Cabibbo-suppressed D decays. Branching fractions are presented for the $K_S K^+$ mode and the previously published $\pi^-\pi^+$ and K^-K^+ modes.[21] We obtain upper limits for the $\pi^+\pi^0$, $\pi^-\pi^+\pi^+$, $K^-K^+\pi^+$, and $\pi^-\pi^-\pi^+\pi^+$ modes.

Great care must be exercised in the detection of Cabibbo-suppressed decays to ensure that Cabibbo-favored decays with misidentified pions or kaons
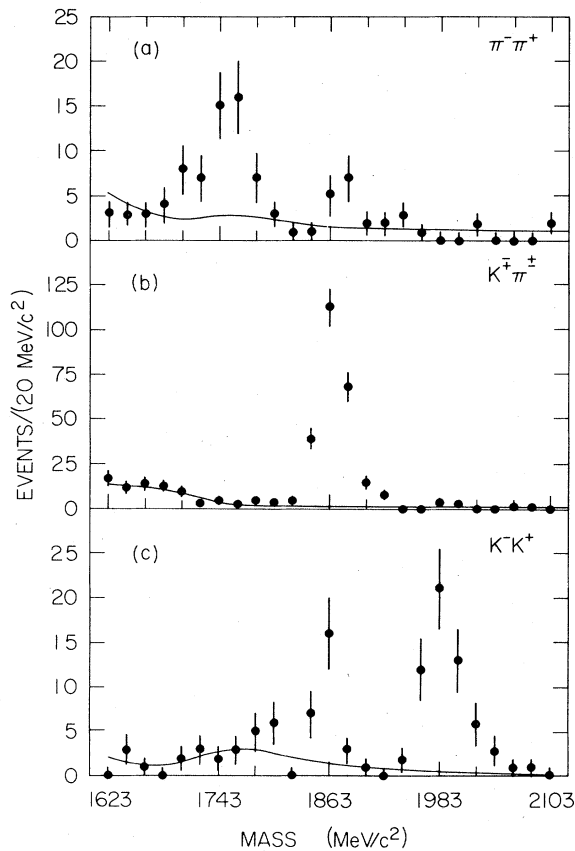
do not contaminate the sample. We generally use a technique which allows the misidentified favored decays to be displayed explicitly. Combinations of particles which are candidates for D decays are required to have momenta within 30 MeV/c of the momentum expected for a D, p_D. All charged particles are required to have good TOF identification. (For the measurement of favored decays, particles which had inconsistent or no TOF measurements were assigned to be pions.) The invariant mass is then computed.

These spectra are shown in Fig. 10 for modes with two charged particles and in Fig. 11 for modes with a K_S and one charged particle. Correctly identified D's appear near the D mass, 1864 MeV/c^2 for D^0's and 1868 MeV/c^2 for D^+'s, while D's in which one particle has been misidentified appear shifted by approximately 120 MeV/c^2 from the D mass. In Fig. 10(b), the dominant $K^-\pi^+$ mode is clear; peaks due to misidentified $K\pi$ decays are present near 1744 and 1984 MeV/c^2 in Figs. 10(a) and 10(c), respectively. A clear $D^0 \to K^-K^+$ signal is present in Fig. 10(c) and there is an excess of $\pi^-\pi^+$ events over background in the D^0 region of Fig. 10(a). Similarly, Fig. 11(a) shows the dom-
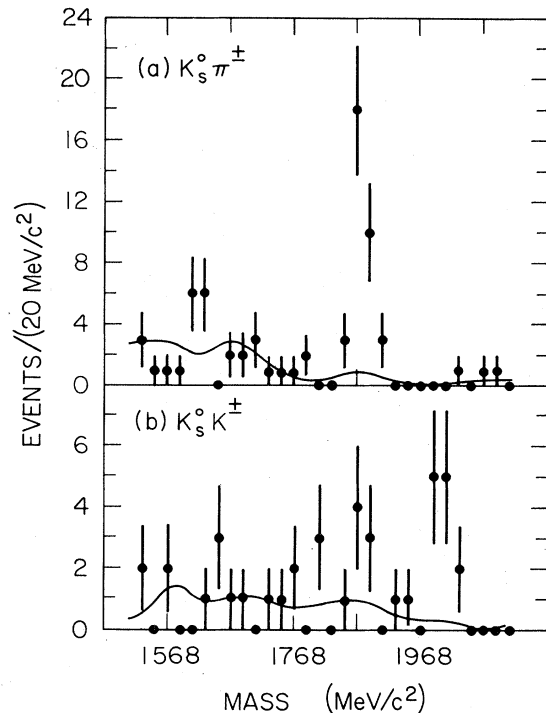

FIG. 10. Invariant-mass spectra for two-particle combinations which have a momentum within 30 MeV/c of the expected D^0 momentum and TOF information consistent with the indicated mode. The curves represent the shapes expected for background events.

FIG. 11. Invariant-mass spectra for K_S^0—charged-particle combinations which have a momentum within 30 MeV/c of the expected D^+ momentum and TOF information consistent with the indicated mode. The curves represent the shapes expected for background events.

inant $K_S \pi^+$ mode, while Fig. 11(b), has an excess of $K_S K^+$ events at the D^+ mass and a peak from misidentified $K_S \pi^+$ events near 1988 MeV/c^2.

To determine the number of signal events, the data of Figs. 10 and 11 are fitted by a maximum-likelihood technique with use of Poisson statistics. The shapes of the background functions used in these fits are derived from control regions with diparticle momenta between 50 and 110 MeV/c higher or lower than p_D. The magnitude of the background is determined both by fits to the data in Figs. 10(a) and 11 and by the number of events in the control regions. These backgrounds are displayed as smooth curves in these figures.

The number of events determined by these fits and the ratios of detection efficiencies and branching fractions between the suppressed and favored modes are given in Table V. The statistical probabilities that the $\pi^- \pi^+$ and $K_S K^+$ signals are purely fluctuations in the background are about 7×10^{-3} and 5×10^{-3}, respectively.

The remaining two-body D^+ mode $\pi^+ \pi^0$ cannot be confused with any misidentified favored mode; the $K^+ \pi^0$ mode has $\Delta C = -\Delta S$ and is doubly Cabibbo suppressed. For this reason, it is analyzed using the same beam-energy constraint techniques discussed in Sec. V A. The mass plot for this mode is shown in Fig. 12. Although there appears to be a small excess of events at the D^+ mass, the significance of the signal is even less than it appears at first glance. A maximum-likelihood fit performed in 1-MeV/c^2 bins using the expected Gaussian resolution function with rms width of 2.2 MeV/c^2 indicates that there is no significant signal. Accordingly, we give only an upper limit in
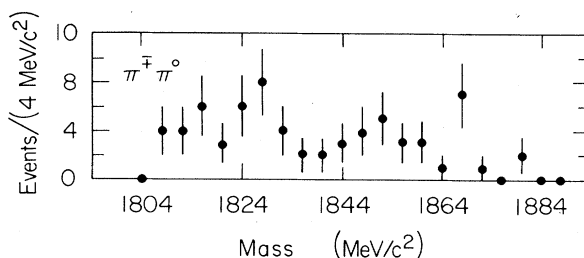

FIG. 12. Beam–energy-constrained mass spectrum for $\pi^+ \pi^0$ combinations.

Table V.

Three- and four-body Cabibbo-suppressed decays are more difficult to observe because of larger combinatorial backgrounds. We have searched for three modes, $\pi^- \pi^+ \pi^+$, $K^- K^+ \pi^+$, and $\pi^- \pi^+ \pi^- \pi^+$. The analysis technique is the same as for the $\pi^- \pi^+$ and $K^- K^+$ modes except that it was necessary to require that no $\pi^- \pi^+$ combination have a mass within 40 MeV/c^2 of the K_S mass to eliminate contamination from the favored $K_S \pi^+$ and $K_S \pi^- \pi^+$ modes. The mass plots are shown in Fig. 13. There is no evidence of any signal so we give upper limits in Table V. The upper limit on the $\pi^- \pi^+ \pi^+$ mode is comparable to the upper limit which was previously measured at higher energy.[14]

D. Mass of the D mesons

In all modes where D signals exist, the mass values agree well with the previously reported values[15] for the neutral and charged states. The observed rms width of about 2.0 MeV/c^2 for each channel is consistent with contributions from the

TABLE V. Measurements on Cabibbo-suppressed D decays. Upper limits are at the 90% confidence level.

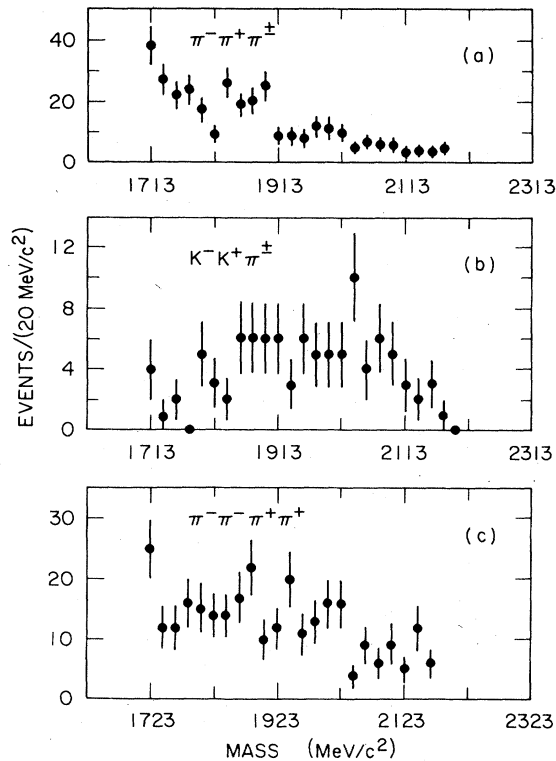| Mode	Number of signal events in the suppressed mode	Ratio of efficiencies	Ratio of branching fractions
$\dfrac{\Gamma(\pi^- \pi^+)}{\Gamma(K^- \pi^+)}$	9.3 ± 3.9	1.19	0.033 ± 0.015
$\dfrac{\Gamma(K^- K^+)}{\Gamma(K^- \pi^+)}$	22.1 ± 5.2	0.84	0.113 ± 0.030
$\dfrac{\Gamma(\pi^0 \pi^+)}{\Gamma(\overline{K}^0 \pi^+)}$	<7.5	1.03	<0.30
$\dfrac{\Gamma(\overline{K}^0 K^+)}{\Gamma(\overline{K}^0 \pi^+)}$	5.6 ± 3.0	0.71	0.25 ± 0.15
$\dfrac{\Gamma(\pi^- \pi^+ \pi^+)}{\Gamma(K^- \pi^+ \pi^+)}$	<21.6	1.12	<0.084
$\dfrac{\Gamma(K^- K^+ \pi^+)}{\Gamma(K^- \pi^+ \pi^+)}$	<18.0	0.56	<0.14
$\dfrac{\Gamma(\pi^- \pi^- \pi^+ \pi^+)}{\Gamma(K^- \pi^- \pi^+ \pi^+)}$	<32.2	1.28	<0.21

FIG. 13. Invariant-mass spectra for three- and four-particle combinations which have a momentum within 30 MeV/c of the expected D momentum, TOF information consistent with the indicated mode, and no $\pi^+\pi^-$ combination within 40 MeV/c^2 of the K^0 mass.

spread in E_b and from momentum resolution. From fits to the signal and background regions in the $K^-\pi^+$ and $K^-\pi^+\pi^+\pi^-$ decays for the D^0 and the $K^-\pi^+\pi^+$ decay for the D^+ we obtain the values for the masses and mass difference shown in Table VI. Table VI also lists the previous measurements.[15] The errors in Table VI contain the uncertainties from the statistics, the momentum calibration, dE/dx corrections, vertex fitting, and beam-energy monitoring. An additional error of 2.5 MeV/c^2 common to both experiments is associated with the SPEAR storage-ring energy calibration. The mass difference is measured more precisely than either mass because many systematic uncertainties cancel. There is also negligible uncertainty due to the storage-ring energy calibration.

VI. INCLUSIVE PROPERTIES OF *D*-MESON DECAYS

In this section we present inclusive measurements of the charged-particle multiplicity and strangeness associated with D^+ and D^0. We also report a new measurement of the individual semileptonic decay fractions of the D^+ and D^0. This

TABLE VI. Mass of D mesons determined by this experiment and by the lead-glass-wall (Mark I) experiment (Ref. 15). The errors include all uncertainties except the 0.13% uncertainty in the SPEAR energy calibration which is common to both experiments. With the SPEAR energy calibration the mass of the ψ is 3095 GeV/c^2, and the D masses will vary proportionally with a variation in the ψ mass.

Measurement	This experiment	Ref. 15
M_{D^0} (MeV/c^2)	1863.8 ± 0.5	1863.3 ± 0.9
M_{D^+} (MeV/c^2)	1868.4 ± 0.5	1868.3 ± 0.9
$M_{D^+} - M_{D^0}$ (MeV/c^2)	4.7 ± 0.3	5.0 ± 0.8

latter measurement is used to determine the ratio of total widths of the charged and neutral D's.

The uniqueness of the $D\bar{D}$ final state at the ψ'' allows us to study "tagged" events. If one D is identified in the $\bar{K}^0\pi^+$, $K^-\pi^+$, $K^-\pi^+\pi^+$, or $K^-\pi^+\pi^+\pi^-$ channel, then the recoiling system is a D meson of known type and momentum. We choose these modes for their excellent signal-to-background ratio and good detection efficiency.

The tagged samples are selected by geometric and TOF cuts similar to those employed in the analysis of Sec. V. Small variations among the tagged sample sizes come from differences in the TOF, π fiducial cuts, and energy constraints required in each of the following analyses. In general we have used a ± 6 MeV/c^2 cut around the constrained D mass, but a tighter cut (± 4 MeV/c^2) is employed for the $K^-\pi^+\pi^+\pi^-$ tags in order to improve the signal-to-background ratio. The data sample includes approximately 300 D^+ and 480 D^0 tags over a background of about 12% of the signal.

A. Multiplicity

The charged-particle multiplicity of D mesons is the simplest measurement that can be made with the tagged sample. For each tagged event, the multiplicity observed in the recoiling system is plotted with no attempt at particle identification. These observed multiplicity distributions are shown in Fig. 14. The cross-hatched area represents an estimate of the background multiplicity distribution obtained from events in the mass band just below the D mass (1800–1855 MeV/c^2) normalized to the expected number of background events contaminating the tagged sample. The produced multiplicity distribution (where K_S^0's are counted as two tracks in their $\pi^+\pi^-$ decay) can be obtained by a numerical unfolding procedure.[34] A solution is sought for the overconstrained system of linear equations
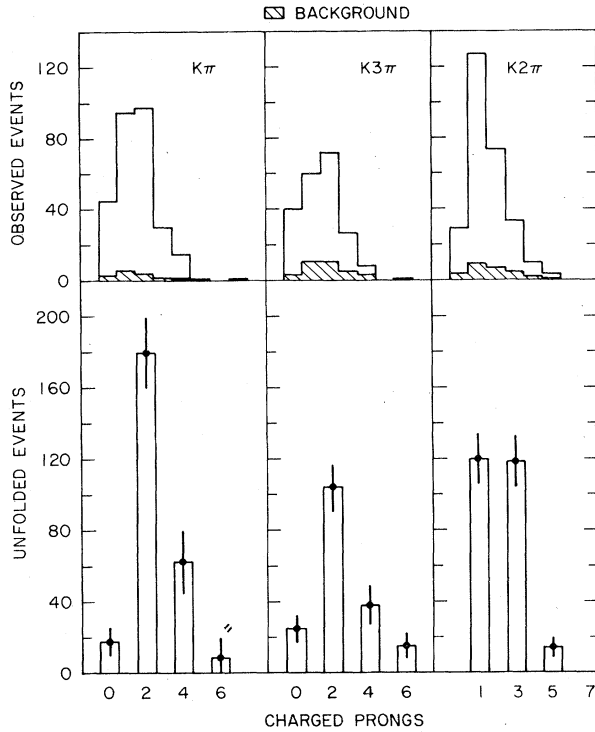
FIG. 14. Charged-particle multiplicity distributions recoiling against the indicated tagging decays. The upper histograms give the observed distributions and the lower histograms give the unfolded distributions. The shaded areas in the upper histograms represent background contributions.

$$\sum_j E_{ij}P_j + B_i = D_i , \qquad (13)$$

where P_j and D_i are vectors containing the produced and detected multiplicities, E_{ij} is a Monte Carlo-generated efficiency matrix whose elements are the probabilities of detecting i particles when j are produced, and B_i is a vector which represents the multiplicity of background events. Equation (13) is solved by a maximum-likelihood technique that employs Poisson statistics. The unfolded distributions are shown in Fig. 14, where the errors reflect only the statistics of the unfolding procedure. The systematic errors are comparable. The mean charged-particle multiplicity is given for the three tagged channels in Table VII.

Systematic errors arise predominantly from uncertainty in the background distribution and from model dependence in the efficiency matrix. Good agreement is observed between the two D^0 channels which have significantly different backgrounds. These results are in good agreement with the previously reported value for the average charged multiplicity of 2.3 ± 0.3 both for D^0 and D^+.[20] Si-

TABLE VII. Charged-particle multiplicities. The first error is statistical and the second is systematic.

Tag	Events	Background	Charged-particle multiplicity
$K^-\pi^+$	283	17	$2.46 \pm 0.12 \pm 0.10$
$K^-\pi^+\pi^+\pi^-$	211	31	$2.48 \pm 0.19 \pm 0.21$
$K^-\pi^+\pi^+$	282	25	$2.16 \pm 0.11 \pm 0.12$

milarly, we find that the multiplicity distributions also coincide well.

B. Strange particles

The tagged samples were chosen to have unique strangeness so that the kaons in the recoiling D could be characterized as having either the same or opposite strangeness. A Cabibbo-favored decay should produce one kaon whose strangeness is opposite that of the tagging decay, while a suppressed decay is expected to exhibit either no strange particle or two particles of opposite strangeness. $D^0\bar{D}^0$ mixing and doubly suppressed decays can also produce equal strangeness in the system, but these are expected to be even smaller sources.[28]

To determine the number of charged kaons, we again use TOF separation on all recoiling particles. Three sources of background are identified and estimated once the TOF separation is made:

(1) Kaons coming from background events contaminating the tagged sample. They are estimated from the events below the D mass (1800–1855 MeV/c^2) and subtracted.

(2) Misidentification of $\pi^\pm$ as $K^\pm$ either through TOF resolution, tracking errors, in-flight decays, or multiple hits in TOF counters. The data are corrected by folding the observed $\pi^\pm$ distribution (of the appropriate charge) with a Monte Carlo calculation of the momentum dependence of the misidentification rate. The correction is found to be small over most of the pion spectrum ($\leq 1\%$ for momenta below 600 MeV/c). The absolute correction varies because of the observed asymmetry in the charge distribution of pions opposite the tags.

(3) The $K^-\pi^+$ tagging channel can be mislabeled as π^-K^+ and still detected as a D meson, with the strangeness then being incorrect. This is found by Monte Carlo to be a 3.3% correction to the $K^-\pi^+$ sample. This expected rate is found to be consistent with an independent determination of the strangeness of the tag using a combination of TOF information and kinematic fitting.

Charged kaons are lost predominantly through their in-flight decay and resulting incorrect momentum and TOF measurement. The inclusive

TABLE VIII. Summary of the inclusive charged-kaon branching-fraction calculations.

	$D^0 \to K^-$	$D^0 \to K^+$	$D^+ \to K^-$	$D^+ \to K^+$
Total tagged sample	541		337	
Background events	60		35	
Net tagged sample	481		302	
Observed $K^\pm$	121	25	26	12
Expected background	4.4 ± 1.6	8.5 ± 1.19	3.4 ± 0.7	4.8 ± 1.3
Detection efficiency	0.44	0.44	0.40	0.40
Branching fraction (%)	55 ± 11	8 ± 3	19 ± 5	6 ± 4

kaon detection efficiency is determined by Monte Carlo calculations using various models of D decays similar to those of Ref. 43. These models were modified to match the observed multiplicity, the ratio of neutral to charged kaons, and the charged-pion and -kaon momentum distributions detected opposite the tags. The variation in detection efficiency was found to be insensitive to these models, with extreme variations amounting to less than 10% of the correction. The results are summarized in Table VIII, where both statistical and systematic errors are included in the final entries.

Neutral kaons are also detected, but their lower detection efficiency and larger backgrounds lead to greater uncertainties in branching ratios. Backgrounds from tagged sample contamination are treated as before using events from lower masses. Additional background arises from random $\pi^+\pi^-$ combinations which create fake K_S^0. This rate is estimated by Monte Carlo simulation in order to properly account for the specific charge correlations and multiplicities. The inclusive K^0 detection efficiencies are found to be 0.090 and 0.095 for D^0 and D^+, respectively, where the branching ratios of K^0 to K_S^0 and K_S^0 to $\pi^+\pi^-$ are included. Model dependence, tracking, and K^0 reconstruction uncertainties lead to a 17% systematic uncertainty in the efficiency. The results are summarized in Table IX where all errors have been included in the final results.

Table X contains a comparison of the results

from Tables VIII and IX with previous measurements done by the lead-glass-wall experiment using the Mark I detector.[20] The results generally agree within the large combined errors.

Totaling the kaon branching fractions from Tables VIII and IX we obtain overall kaon multiplicities of 0.92 ± 0.16 and 0.77 ± 0.19 for D^0 and D^+, respectively. However, these kaons cannot all be attributed to the Cabibbo-favored charm to strange-quark transition illustrated in Fig. 1, since a significant fraction have the wrong strangeness. An interesting and well-defined quantity is the net strangeness in D decays. It can be computed from our measurements with one assumption which is subject to considerable error, namely, that there are equal numbers of charged and neutral kaons with the wrong strangeness. Assuming this, the net values of strangeness in D^0 and D^+ decay products are -0.60 ± 0.20 and -0.53 ± 0.22, respectively. These values are 1.5 and 1.7 standard deviations below the value of -0.90 expected in the naive model.

C. Semileptonic decays

Because the Cabibbo-allowed semileptonic decay amplitude has $\Delta I = 0$, the corresponding semileptonic partial widths for the two members of the D isodoublet are expected to be equal. Therefore, a measurement of the relative D^0 and D^+ semileptonic branching fractions using tagged events determines the ratio of lifetimes of the two species, assuming that they are almost exclusively

TABLE IX. Summary of the inclusive neutral-kaon branching-fraction calculation.

	$D^0 \to \bar{K}^0$ or K^0	$D^+ \to \bar{K}^0$ or K^0
Total tagged sample	541	337
Background events	60	35
Net tagged sample	481	302
Observed K_S	17	18
Background in the tagged sample	1.5 ± 0.5	1.2 ± 0.5
Combinatorial background	2.9 ± 1.0	1.8 ± 0.8
Net K_S	12.6 ± 4.3	15.0 ± 4.3
Detection efficiency	0.090	0.095
Branching fraction (%)	29 ± 11	52 ± 18

TABLE X. Comparison of strange-particle branching fractions measured by this experiment and the lead-glass-wall (Mark I) experiment (Ref. 20).

		D^0 (%)	D^+ (%)
$B(D \to K^-)$	This experiment	55 ± 11	19 ± 5
	Ref. 20	36 ± 10	10 ± 7
$B(D \to K^+)$	This experiment	8 ± 3	6 ± 4
	Ref. 20		6 ± 6
$B(D \to \bar{K}^0$ or K^0	This experiment	29 ± 11	52 ± 18
	Ref. 20.	57 ± 26	39 ± 29

Cabibbo allowed.[44,45]

We search the tagged events for electrons in the recoil system using TOF and calorimeter information. Candidate tracks are first selected by the usual geometric cuts, and are required to have both a good TOF measurement and a momentum greater than 100 MeV/c. All tracks having kaon weight > 0.05 are removed. This cut removes less than 3% of the tracks previously labeled pions, and effectively removes all recoiling $K^{\pm}$. For tracks with momenta less than 300 MeV/c, TOF is used to classify them as π or e. A track is called an electron if the electron weight under the π-e hypothesis exceeds 0.90. The hadron misidentification rate ranges from 3% to 7% for track momenta from 100 to 300 MeV/c, while the efficiency for electron identification drops from 86% to 62% in this range. For tracks with momenta greater than 300 MeV/c, a combination of TOF and calorimeter information is used to classify them employing a technique described in Ref. 46. The algorithm takes 23 measured quantities for each track such as TOF, momentum, angle of incidence, and energy deposition and transverse shower spread at 7 depths in the lead-liquid-argon calorimeter stack, and selects regions of this multidimensional space that are distinctly populated by electrons or pions. These regions are established using pure samples of electrons selected from photon conversions and radiative Bhabha-scattering events, and pions from K_S^0 and $\psi(3095)$ decays. Classification and misidentification rates are determined from the data by setting aside a random sample of these pure events, and testing them after the selection criteria are established. For candidate tracks with momenta ranging from 300 to 1000 MeV/c, hadron misidentification drops from 7.8% to 3.5% while the electron efficiency rises from 67% to 85%. The moderately low electron efficiency from 300 MeV/c to about 500 MeV/c comes from the diminishing TOF separation and the onset of calorimetric separation. Poorer efficiency is traded for a reasonably small hadron misidentification rate.

Fifty-nine D^0 events and 50 D^+ events contained identified electrons. These events were hand scanned to remove visible photon conversions in the beam pipe and surrounding material. Five D^0 and seven D^+ events were eliminated for this reason. Photon conversions were identified as two tracks with an opening angle of less than 10°, one of which was identified as an electron and the other of which was consistent with being an electron.

The remaining electrons were separated by charge relative to the strangeness of the tagging decay. We designate those with the expected charge (that is, equal to the strangeness of the tagging decay) as "right"-sign candidates and those with the opposite charge as "wrong"-sign candidates.
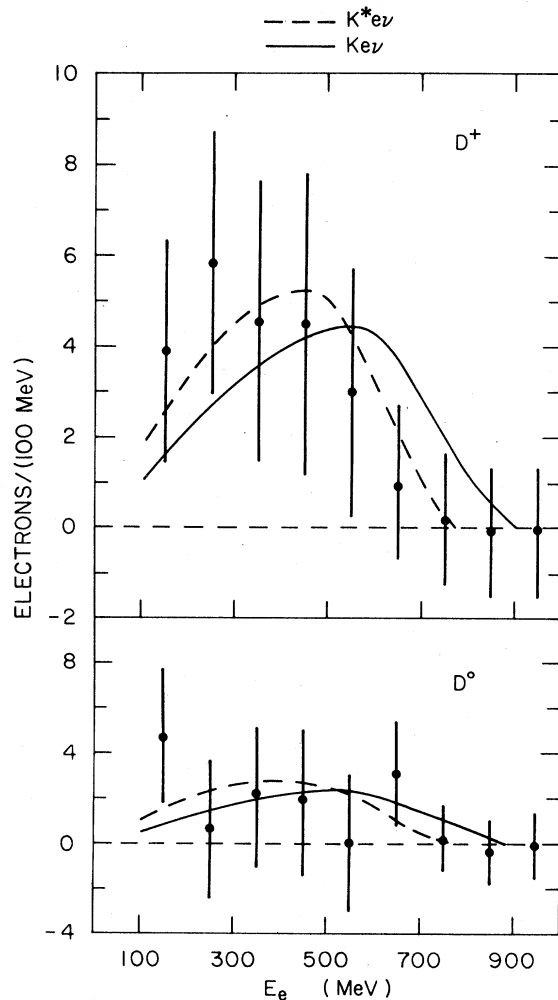

FIG. 15. The corrected (net) electron energy spectra recoiling against D^+ and D^0 tagging decays. The curves indicate the theoretically expected spectra from $D \to Ke\nu$ (solid) and $D \to K^*e\nu$ (dashed) decay modes, normalized to the total number of events.

Four sources of contamination were estimated.

(a) Backgrounds arising from hadron misidentification are not charge symmetric, but depend on the strangeness of the tagging decay. This is particularly evident in charged-D decay due to the excess of right-sign charge, but also occurs in neutral-D decay due to the difference between pion and kaon momentum spectra. The momentum spectra of all tracks recoiling against a tagging decay were folded with the known misidentification rates to estimate the number of electrons expected to be mislabeled in each group.

(b) There are residual backgrounds from asymmetric photon conversions and π^0 Dalitz decays that could not be subtracted in the hand scan. These are charge symmetric so we have estimated them by subtracting the number of wrong-sign electrons that remain after the subtraction for hadron misidentification from the number of right-sign electrons.[47]

(c) Contamination from leptonic kaon decays is estimated to contribute less than 0.3 and 0.05 electrons to the D^0 and D^+ samples, respectively.

(d) Contamination of the tagged sample and π-K interchange in the $K^-\pi^+$ tag sample were discussed previously. Lower-mass events are used to estimate the former, and an appropriate correction is made for the latter.

A summary of the semileptonic decay calculations is given in Table XI. The penultimate entries in the table give a net signal of approximately 12 electrons from D^0 decay and 23 electrons from D^+ decay. The momentum spectra of these electrons is shown in Fig. 15 along with curves that indicate the expected shape of the spectra for D decays

into the $Ke\nu$ and $K^*e\nu$ modes.[48] The theoretical curves are normalized to the total data. The data are consistent with coming from a combination of these two modes, in agreement with the findings of other experiments.[13,17,22] The additional charged-particle multiplicity associated with electrons in the tagged events is also consistent with the hypothesis of semileptonic decays occurring in these two modes.[34]

We obtain the individual D^+ and D^0 semileptonic branching fractions by estimating the inclusive electron efficiency. A Monte Carlo calculation for the $Ke\nu$ and $K^*e\nu$ modes gives an average efficiency of 0.47. We find that this value is not sensitive to either the exact form of the electron spectrum or associated hadronic multiplicity. The results are given in Table XI. The uncertainties in the semileptonic branching fractions are dominated by statistics, but the error estimate includes a systematic uncertainty of about 25%.

Weighting the semileptonic branching fractions by the inclusive D-production cross sections (Eq. 6), we obtain an average branching fraction to electrons of $(10.0 \pm 3.2)\%$. This is comparable with the inclusive measurements of $(7.2 \pm 2.8)\%$ (Ref. 19) and $(8.0 \pm 1.5)\%$ (Ref. 22) by other experiments at the same center-of-mass energy.

We have performed a maximum-likelihood fit to the ratio of the semileptonic branching fractions employing Poisson statistics. Figure 16 shows the negative logarithm of the likelihood function plotted against the ratio of D^+ and D^0 semileptonic rates. By evaluating a ratio, we reduce the systematic error to $\pm 16\%$ (where 5% is from the determination of the hadron misidentification rates,

TABLE XI. Summary of the D semileptonic-decay branching-fraction calculations.

|	D^0			D^+	
Total tagged sample	536			330	
Background	59			35	
Net tagged sample	477			295	
	Right sign		Wrong sign	Right sign	Wrong sign
Observed electrons	36		18	39	4
Expected from hadron misidentification	17.4 ± 1.0		11.8 ± 0.9	16.3 ± 1.0	4.2 ± 0.5
Electrons after subtraction for hadron misidentification	18.6 ± 6.1		6.2 ± 4.3	22.7 ± 6.3	$0^{+2.1}_{-0.0}$
Net right-sign electrons (right sign − wrong sign)		12.4 ± 7.5			22.7 ± 6.6
Net contribution from leptonic K decays, $K^-\pi^+$ mislabeling, and false tags		-0.1 ± 1.0			$+0.6 \pm 0.8$
Net electrons		12.3 ± 7.6			23.3 ± 6.7
Semileptonic branching fraction (%)		5.5 ± 3.7			16.8 ± 6.4
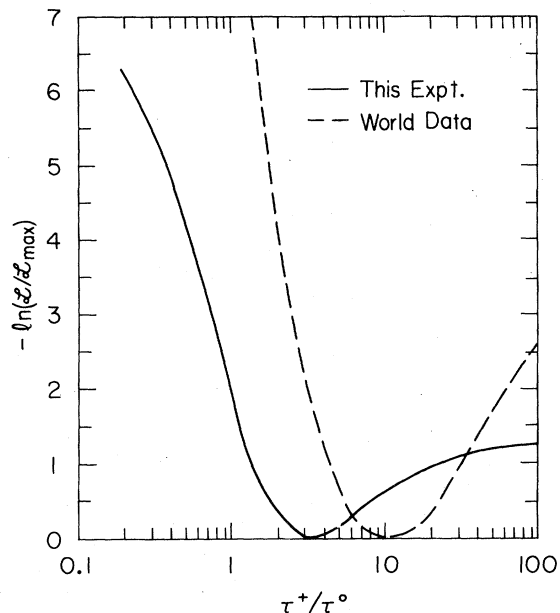
FIG. 16. The negative logarithm of the ratio of likelihood function to its maximum value for this experiment (solid) and for the combination of this experiment, Ref. 3, and Ref. 23 (dashed).

7% is from the hand scanning, and 13% is from the background representation). Since the ratio of rates represents the relative D^+ and D^0 lifetimes (τ_{D^+}/τ_{D^0}), we include these systematic errors with the dominant statistical errors estimated from the shape of the likelihood function about its minimum to obtain

$$\tau_{D^+}/\tau_{D^0} = 3.1^{+4.6}_{-1.4}. \tag{14}$$

The errors here represent one standard deviation about 3.1, assuming a local Gaussian form for the likelihood function. Statistically, a change of about two standard deviations is required to obtain equal lifetimes. The upper limit of τ_{D^+}/τ_{D^0} is poorly defined because of the relatively large error on the small number of D^0 semileptonic decays observed.

Two other experiments have made significant measurements of the ratio of D^+ to D^0 lifetimes. The DELCO experiment has used the measurement of double- and single-electron events from ψ'' decays to obtain[23]

$$\tau_{D^+}/\tau_{D^0} > 4.3 \tag{15}$$

at the 95% confidence level.

Direct measurements of D^0 and D^+ lifetimes in emulsions exposed to neutrino beam yield[3]

$$\tau_{D^+} = (10.3^{+10.5}_{-4.1}) \times 10^{-13} \text{ sec} \tag{16}$$

based on 5 events, and

$$\tau_{D^0} = (1.00^{+0.52}_{-0.31}) \times 10^{-13} \text{ sec} \tag{17}$$

based on 7 events.

Multiplying the likelihood functions from these three experiments together, we obtain the joint likelihood function for the world data shown by the dotted line in Fig. 16.[49,50] At the 1-standard-deviation level, the result is

$$\tau_{D^+}/\tau_{D^0} = 10.0^{+12.0}_{-4.6}. \tag{18}$$

Equality of the two lifetimes is excluded by more than 4 standard deviations.

VII. DISCUSSION

In the most general terms the properties of D decays agree well with what was expected from the GIM current.[26] The existence of an isodoublet of D mesons, the strangeness content of their dominant decays, and the existence of Cabibbo-suppressed decays with roughly the proper magnitude of suppression all attest to the correctness of the original hypothesis.

However, the details of D decays do not always agree with the perhaps naive picture of theoretical expectations that we sketched in Sec. II. The most basic discrepancy is the inequality of D^0 and D^+ lifetimes. Branching fractions for specific decay modes are not in agreement with simple models. In particular the ratio $B(D^0 \to \bar{K}^0\pi^0)/B(D^0 \to K^-\pi^+)$ is not small and the ratio $B(D^0 \to K^-K^+)/B(D^0 \to \pi^-\pi^+)$ is not unity.

A large number of theoretical papers have attempted to modify the simple models in order to explain some of these results. It is not our purpose here to review this vast literature.[51] We will, however, sketch some of the major ideas and indicate, where appropriate, how our measurements are relevant to them.

It was suggested some time ago that nonexotic states might be enhanced relative to exotic states.[28,52,53] This would lead to a longer relative D^+ lifetime since all Cabibbo-favored D^+ decays are exotic. Two broad categories of enhancement techniques have been proposed. The first is the use of the W-exchange diagram, shown in Fig. 17(a) which contributes to D^0 but not D^+ decays. This diagram is suppressed by a factor $(m_u^2 f_D^2/m_c^4)$ because of the helicity of the light quarks and the probability of annihilation. However, it is argued that this suppression can be circumvented either by the emission of a gluon[54] or by a consideration of the gluon content of the initial state.[55]

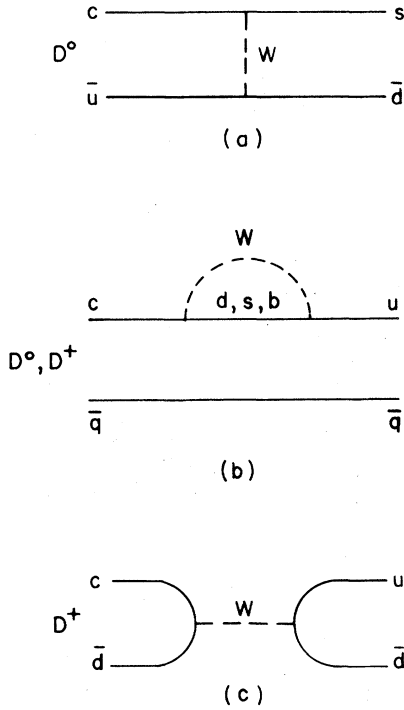The exchange diagram leads to an $I = \frac{1}{2}$ final state for which

FIG. 17. Additional diagrams which can contribute to D decays. (a) Exchange diagram for D^0 Cabibbo-favored decays. (b) Penguin diagram for D^0 and D^+ Cabibbo-suppressed decays. (c) Annihilation diagram for D^+ Cabibbo-suppressed decays.

$$\frac{B(D^0 \to K^-\pi^+)}{B(D^0 \to \overline{K}^0\pi^0)} = \frac{B(D^0 \to K^{*-}\pi^+)}{B(D^0 \to \overline{K}^{*0}\pi^0)}$$

$$= \frac{B(D^0 \to K^-\rho^+)}{B(D^0 \to \overline{K}^0\rho^0)} = 2 . \qquad (19)$$

Tables I and IV indicate that the data are consistent with the first two relationships, but not the last.

The second category of enhancement techniques assumes the spectator diagram (Fig. 1) to be dominant, but requires f^-/f^+ to be larger than the leading-logarithm value and requires that gluon interactions do not change the color structure of the final state.[56,57] In this model the D^+ non-leptonic decay rate is suppressed by a destructive interference between the normal diagram and its Fierz rearrangement. This interference occurs in D^+ decay where the two diagrams lead to identical final states, but not in D^0 decay where they lead to distinct final states. The ratio of D lifetimes in this picture is [56]

$$\frac{\tau_{D^+}}{\tau_{D^0}} = \frac{f_-^2 + 2f_+^2 + 2}{4f_+^2 + 2} . \qquad (20)$$

A value of $f_- = f_+^{-2} = 5$ will yield $\tau_{D^+}/\tau_{D^0} \approx 10$.

One testable prediction in which f_-, or sextet, dominance does not coincide with the prediction of a $I = \frac{1}{2}$ final state occurs in D^+ decay. Assuming SU(3) symmetry and the complete dominance of the part of the amplitude which transforms as a sextet,[58]

$$\frac{B(D^+ \to \overline{K}^{*0}\pi^+)}{B(D^+ \to \overline{K}^0\rho^+)} = 1 . \qquad (21)$$

The Mark II data alone [Eqs. (8) and (11)] are compatible with this prediction but the combination of the Mark II measurements and the world data for τ_{D^+}/τ_{D^0} [Eqs. (8) and (12)] are inconsistent with it.

The observation that $B(D^0 \to K^-K^+) \neq B(D^0 \to \pi^-\pi^+)$, contrary to the SU(3) prediction, Eq. (4), has generated a great deal of theoretical discussion. The lack of equality between these two Cabibbo-suppressed decays has been discussed in terms of final-state interactions,[59,60] quark-mass effects,[59,61,62] six-quark mixing angles,[61,63] penguin diagrams [Fig. 17(b)],[59,64,65] right-handed currents,[66] and coupling to charged Higgs bosons.[67]

It has been suggested theoretically that D^+ Cabibbo-suppressed decays may be enhanced relative to Cabibbo-favored decays either because there is an additional diagram for the suppressed decays, Fig. 17(c),[62] or because the sextet-dominance interference does not occur for all suppressed decays.[67] Our data are not conclusive on this issue. One indication of a potentially large D^+ Cabibbo-suppressed decay rate is the measurement in Sec. VI B of net strangeness of -0.53 ± 0.22 in D^+ decay. On the other hand, we have seen no conclusive evidence of large exclusive D^+ Cabibbo-suppressed decay modes. The $D^+ \to \overline{K}^0K^+$ to $D^+ \to \overline{K}^0\pi^+$ ratio may not be typical since the $D^+ \to \overline{K}^0\pi^+$ mode is suppressed in any model because it has no sextet component.[58] However, the $D^+ \to \pi^-\pi^+\pi^+$ mode is expected to be typical of D^+ Cabibbo-suppressed decays.[62,68] The upper limit from Table III,

$$\frac{B(D^+ \to \pi^-\pi^+\pi^+)}{B(D^+ \to K^-\pi^+\pi^+)} < 0.084 , \qquad (22)$$

at the 90% confidence level, and a similar limit from a previous experiment[14] appear quite constrictive.

ACKNOWLEDGMENTS

---

*Present address: CERN, Geneva, Switzerland.

†Present address: Vanderbilt University, Nashville, Tenn. 37235.

‡Present address: California Institute of Technology, Pasadena, Calif. 91125.

§Present address: Harvard University, Cambridge, Mass. 02138.

‖Present address: Universität Bonn, Federal Republic of Germany.

¶Present address: CEN-Saclay, France.

**Present address: DESY, Hamburg, Federal Republic of Germany.

††Present address: Laboratoire de Physique Nucléaire et Hautes Energies, École Polytechnique, Palaiseau, France.

[1]G. Goldhaber *et al.*, Phys. Rev. Lett. 37, 255 (1976); I. Peruzzi *et al.*, *ibid.* 37, 569 (1976).

[2]C. Baltay *et al.*, Phys. Rev. Lett. 41, 73 (1978).

[3]N. Ushida *et al.*, Phys. Rev. Lett. 45, 1049 (1980); 45, 1053 (1980).

[4]J. Blietschau *et al.*, Phys. Lett. 86B, 108 (1979).

[5]D. Drijard *et al.*, Phys. Lett. 81B, 250 (1979).

[6]M. S. Atiya *et al.*, Phys. Rev. Lett. 43, 414 (1979).

[7]M. I. Adamovich *et al.*, Phys. Lett. 89B, 427 (1980).

[8]D. Alston *et al.*, Phys. Lett. 94B, 113 (1980).

[9]J. E. Wiss, *et al.*, Phys. Rev. Lett. 37, 1531 (1976).

[10]G. J. Feldman *et al.*, Phys. Rev. Lett. 38, 1313 (1977).

[11]H. K. Nguyen *et al.*, Phys. Rev. Lett. 39, 262 (1977).

[12]G. Goldhaber *et al.*, Phys. Lett. 69B, 503 (1977).

[13]R. Brandelik *et al.*, Phys. Lett. 70B, 387 (1977).

[14]M. Piccolo *et al.*, Phys. Lett. 70B, 260 (1977).

[15]I. Peruzzi *et al.*, Phys. Rev. Lett. 39, 1301 (1977).

[16]D. L. Scharre *et al.*, Phys. Rev. Lett. 40, 74 (1978).

[17]J. M. Feller *et al.*, Phys. Rev. Lett. 40, 274 (1978).

[18]W. Bacino *et al.*, Phys. Rev. Lett. 40, 671 (1978).

[19]J. M. Feller *et al.*, Phys. Rev. Lett. 40, 1677 (1978).

[20]V. Vuillemin *et al.*, Phys. Rev. Lett. 41, 1149 (1978).

[21]G. S. Abrams *et al.*, Phys. Rev. Lett. 43, 481 (1979).

[22]W. Bacino *et al.*, Phys. Rev. Lett. 43, 1073 (1979).

[23]W. Bacino *et al.*, Phys. Rev. Lett. 45, 329 (1980).

[24]P. A. Rapidis *et al.*, Phys. Rev. Lett. 39, 526 (1977).

[25]R. H. Schindler *et al.*, Phys. Rev. D 21, 2716 (1980).

[26]S. L. Glashow, J. Illiopoulos, and L. Maiani, Phys. Rev. D 2, 1285 (1970).

[27]J. D. Bjorken and S. L. Glashow, Phys. Lett. 11, 255 (1964).

[28]M. K. Gaillard, B. W. Lee, and J. L. Rosner, Rev. Mod. Phys. 47, 277 (1975).

[29]G. Altarelli, N. Cabibbo, and L. Maiani, Nucl. Phys. B88, 285 (1975); R. L. Kingsley, S. B. Treiman, F. Wilczek, and A. Zee, Phys. Rev. D 11, 1919 (1975).

[30]J. Ellis, M. K. Gaillard, and D. V. Nanopoulos, Nucl. Phys. B100, 313 (1975).

[31]D. Fakirov and B. Stech, Nucl. Phys. B133, 315 (1978).

[32]N. Cabibbo and L. Maiani, Phys. Lett. 73B, 418 (1978).

[33]M. Kobayashi and K. Maskawa, Prog. Theor. Phys.

49, 652 (1973).

[34]R. H. Schindler, Ph.D. thesis, SLAC Report No. SLAC-219, 1979 (unpublished).

[35]W. Davies-White *et al.*, Nucl. Instrum. Methods 160, 227 (1979).

[36]H. Brafmann *et al.*, IEEE Trans. Nucl. Sci. NS25, 692 (1978); M. Breidenbach *et al.*, *ibid.* NS25, 706 (1978).

[37]G. S. Abrams *et al.*, IEEE Trans. Nucl. Sci. NS25, 309 (1978); NS27, 59 (1980).

[38]G. S. Abrams *et al.*, Phys. Rev. Lett. 44, 10 (1980).

[39]R. L. Ford and W. R. Nelson, SLAC Report No. SLAC-210, 1980 (unpublished).

[40]B. Jongejans, in *Methods in Subnuclear Physics*, edited by M. Nikolic (Gordon and Breach, New York, 1970), Vol. IV.

[41]The number of events in this section differs slightly from the values given in Table I due to different selection criteria.

[42]Earlier results from the Mark I detector (Ref. 9) indicated consistency with a uniform Dalitz-plot distribution. This experiment had a D^* sample approximately four times smaller, which contained an almost equal number of signal and background events.

[43]C. Quigg and J. L. Rosner, Phys. Rev. D 17, 239 (1978).

[44]A. Pais and S. B. Treiman, Phys. Rev. D 15, 2539 (1977).

[45]M. Peshkin and J. L. Rosner, Nucl. Phys. B122, 144 (1977).

[46]J. H. Friedman, IEEE Trans. Comput. C26, 404 (1977).

[47]Energetic knock-on electrons are not a background because the hadrons from D decay have insufficient energy to eject a 100-MeV/c electron. However, if they were a background they would be subtracted by this procedure since they are charge symmetric with respect to the strangeness of the tagging decay.

[48]A. Ali and T. C. Yang, Phys. Lett. 65B, 275 (1976).

[49]We are grateful to G. Donaldson for preparing likelihood functions for the DELCO data and for useful discussions.

[50]N. Ushida *et al.*, Ohio State University Reports Nos. DOE/ER/01545-277 and DOE/ER/01545-278 1980 (unpublished). Abridged versions of these reports were published as Ref. 3 without the likelihood-function plots.

[51]Recent reviews are M. S. Chanowitz, in *High Energy e^+e^- Interactions*, proceedings of the International Symposium, Vanderbilt University, 1980, edited by R. S. Panvini and C. S. Csorna (AIP, New York, 1980); D. G. Hitlin, in Proceedings of the 1980 SLAC Summer Institute on Particle Physics (unpublished).

[52]T. Hayashi *et al.*, Prog. Theor. Phys. 49, 351 (1973); 52, 636 (1974).

[53]E. Ma, S. Pakvasa, and W. Simmons, Z. Phys. C 5, 309 (1980); M. Matsuda, M. Nakagawa, and S. Ogawa, Prog. Theor. Phys. 63, 351 (1980); I. Bigi and L. Stodolsky, SLAC Report No. SLAC-PUB-2410, 1979 (un-

published).

[54]M. Bander, D. Silverman, and A. Soni, Phys. Rev. Lett. 44, 7 (1980). But see also M. Suzuki, Nucl. Phys. B177, 413 (1981) and J. Finjord, University of Bern report, 1980 (unpublished).

[55]H. Fritzsch and P. Minkowski, Phys. Lett. 90B, 455 (1980).

[56]B. Guberina et al., Phys. Lett. 89B, 111 (1979).

[57]M. Katuya and Y. Koide, Phys. Rev. D 19, 2631 (1979).

[58]M. B. Einhorn and C. Quigg, Phys. Rev. D 12, 2015 (1975).

[59]J. F. Donoghue and B. R. Holstein, Phys. Rev. D 21, 1334 (1980).

[60]H. J. Lipkin, Fermilab Report No. FERMILAB-PUB-79/84-THY, 1979 (unpublished); D. G. Sutherland, Phys. Lett. 90B, 173 (1980).

[61]V. Barger and S. Pakvasa, Phys. Rev. Lett. 43, 812 (1980).

[62]H. Fritzsch and P. Minkowski, Nucl. Phys. B171, 413 (1980).

[63]M. Suzuki, Phys. Rev. Lett. 43, 818 (1979); L.-L. C. Wang and F. Wilczek, ibid. 43, 816 (1979).

[64]M. Glück, Phys. Lett. 88B, 145 (1979); K. Ishikawa, UCLA Reports Nos. UCLA/79/TEP/11 and UCLA/79/TEP/20, 1979 (unpublished); M. Fukugita, T. Hagiwara, and A. I. Sanda, Rutherford Laboratory Report No. RL-79-052, 1979 (unpublished).

[65]L. F. Abbot, P. Sikivie, and M. B. Wise, Phys. Rev. D 21, 768 (1980).

[66]Y. Abe et al., Nuovo Cimento A56, 345 (1980); R. C. Verma and A. N. Kamal, University of Alberta report, 1979 (unpublished).

[67]I. I. Y. Bigi, Phys. Lett. 90B, 177 (1980).

[68]F. J. Gilman has emphasized the importance of this mode in a talk at the DESY Workshop on Flavor Dynamics, Hamburg, Germany, 1980 (unpublished).